This is a repository copy of *Intracellular delivery of nano-formulated antituberculosis drugs enhances bactericidal activity*.

White Rose Research Online URL for this paper:
http://eprints.whiterose.ac.uk/156860/

Version: Published Version

ORIGINAL ARTICLE

Intracellular delivery of nano-formulated antituberculosis drugs enhances bactericidal activity

Samantha Donnellan,[1,2,4*] (iD) Vicki Stone,[2] Helinor Johnston,[2] Marco Giardiello,[3] Andrew Owen,[3] Steve Rannard,[3] Ghaith Aljayyoussi,[4] Benjamin Swift,[5] Lang Tran,[6] Craig Watkins[1] & Karen Stevenson[1*]

[1] *Moredun Research Institute, Pentlands Science Park, Bush Loan, Penicuik EH26 0PZ, UK*

[2] *School of Engineering and Physical Sciences, Institute of Biological Chemistry, Biophysics and Bioengineering, Heriot-Watt University, Riccarton, Edinburgh EH14 4AS, UK*

[3] *Department of Chemistry, University of Liverpool, Crown Street, Liverpool L69 3BX, UK*

[4] *Research Centre for Drugs and Diagnostics, Liverpool School of Tropical Medicine, Liverpool L3 5QA, UK*

[5] *School of Veterinary Medicine and Science, University of Nottingham, Loughborough LE12 5RD, UK*

[6] *Institute of Occupational Medicine, Research Avenue North, Riccarton, Edinburgh EH14 4AP, UK*

Abstract

Tuberculosis kills more people worldwide than any other infectious disease. Treatment requires multiple drug therapy administered over long periods (6-24 months). The emergence of multidrug-resistant strains is a major problem, and with few new drugs in the pipeline, a novel modus operandi is urgently required. Solid drug nanoparticles (SDNs), a new development in nanomedicine, offer a fresh therapeutic approach. Here, we show that SDNs are more effective (50-fold) at killing pathogenic mycobacteria than aqueous forms of the same drug and can target mycobacteria internalised by macrophages, where bacilli reside. We demonstrate synthesis of dual and triple drug loaded SDNs, facilitating combination tuberculosis therapy. Our results suggest that by employing SDNs of existing antibiotics, it may be possible to improve drug delivery and therefore reduce drug dosage to lessen side effects and fight drug resistance.

Introduction

The use of nanoparticles (NPs) for drug delivery systems is an expanding area of research (Vadakkan *et al.* 2013; Pedrosa *et al.* 2014; Choudhary and Kusum Devi 2015; Patel *et al.* 2013). The antimicrobial properties of some NPs are well documented (Donnellan *et al.* 2015; Owens 2013; Neyrolles *et al.* 2013; Bondarenko *et al.* 2012; Mohanty *et al.* 2013), offer increased bioavailability (Pandey and Khuller 2005; Mcdonald *et al.* 2014), and may allow targeted treatment (Wang *et al.* 2014), and NPs show promise against other diseases such as the human

immunodeficiency virus (HIV) (Mcdonald *et al*. 2014; Williams *et al*. 2015).

Solid drug nanoparticles (SDNs) are a novel development in nanotechnology (Mcdonald *et al*. 2014). They are not a drug carrier system; they are nano-sized amorphous particles, constructed of active pharmaceutical ingredients (APIs) (Siccardi *et al*. 2016). There are many advantages to creating excipient stabilised nanoparticulate versions of FDA-approved therapeutics, for example, they use existing APIs, thus saving time and the exorbitant costs involved in novel drug development and testing, they increase bioavailability, and they may offer an opportunity to lower treatment dose.

Tuberculosis (TB), caused by *Mycobacterium tuberculosis* (*Mtb*), kills up to 2 million people each year with one third of the world's population estimated to have latent TB (WHO 2016). Drug-resistant strains and the susceptibility to TB infection of HIV patients heighten this global crisis, compounded by the development of very few drugs in the past 40 years (WHO 2014; WHO 2015; WHO 2016). Treatment periods are very long (6–24 months) requiring multiple drug administration, which is highly expensive and often unsuccessful because of patient noncompliance. Current treatment typically involves an initial four-drug regimen: rifampicin (RIF), isoniazid (INH), pyrazinamide (PZA), and ethambutol (WHO 2016; Pandey and Ahmad 2011).

Herein, we describe the manufacture of anti-TB SDNs and hypothesise that the delivery of existing antibiotics in the form of SDNs would enhance toxicity to mycobacteria and facilitate delivery to intracellular compartments due to colocalisation following phagocytic uptake.

Experimental Section

Aqueous drug preparation

Rifampicin and INH were purchased from Sigma-Aldrich® (Poole, UK) and prepared (and stored) following product documentation. Stock solutions were stored in tin-foil wrapped bottles at 4°C. From these stock solutions, appropriate serial dilutions were made in Middlebrook 7H9 broth for the desired concentrations.

SDN manufacture

Solid drug nanoparticles of first line TB drugs were prepared similarly to Mcdonald *et al*. (2014) as outlined later. The incorporation of a fluorescent dye (1,1′-dioctadecyl-3,3,3′,3′-tetramethylindodicarbocyanine, 4-chlorobenzenesulfonate salt (DiD)) to confer a fluorescent signal to each particle was included in some incidences for imaging purposes. Both freeze and spray drying methods were used, essentially producing the same NP dispersions, while spray drying only was used to scale up the samples as freeze drying could only produce relatively small quantities (up to 10 mg).

Preparation of emulsion-templated freeze-dried monoliths containing 30% RIF nanoparticles (RIF SDN)

Stock solutions of RIF (30 mg/mL in dichloromethane (DCM)), Pluronic F68® (22.5 mg/mL in water), and Hyamine® (22.5 mg/mL in water) were prepared. The three stock solutions were combined in the ratio 100:245:67 (μL) (RIF : Pluronic F68® : Hyamine®) plus 88-μL water. The final solid mass ratio was therefore 30% RIF : 55% Pluronic F68® : 15% Hyamine® in a 1:4 DCM to water mixture (total volume 0.5 mL). The sample was emulsified using a Covaris S2x acoustic homogenisation system for 30 sec with a duty cycle of 20, an intensity of 10, and 500 cycles/burst in frequency sweeping mode. Immediately after emulsification, the sample was cryogenically frozen and lyophilised using a Virtis benchtop K freeze-drier for 48 h. The orange, dry, porous resultant product was stored in the dark at room temperature.

Preparation of emulsion-templated freeze-dried monoliths containing 29% RIF nanoparticles labelled with 1% of the dye DiD (RIF SDN + DiD)

Preparation followed the same procedure as described previously; however, a stock solution of 30-mg/mL DiD was prepared. The four stock solutions were added to a sample tube in the ratio 97:3:267:133 (μL) (RIF : DiD : Pluronic F68® : Hyamine®) plus 88-μL water. The final solid mass ratio was therefore 29% RIF : 1% DiD : 55% Pluronic F68® : 15% Hyamine® in a 1:4 DCM to water mixture, with a total volume of 0.5 mL.

Preparation of emulsion-spray-dried 53% TRIPLE drug powders containing RIF, INH, PZA (TRIPLE SDN)

A mass of 51.2-mg PZA, 20-mg RIF, and 8.8-mg INH were weighed directly into a sample vial. A volume of 1-mL DCM was then added and the powders mixed (inverted and vortexed). Stock solutions of Kollicoat® Protect (22.5 mg/mL in water) and Hyamine® (22.5 mg/mL in water) were dissolved. The aqueous stock solutions were added to the 1-mL API mix in DCM in the ratio 267:0.44 (mL) plus 0.89-mL water. The final solid mass ratio was therefore 34% PZA, 13% RIF : 6% INH : 40%

Kollicoat® Protect : 7% Hyamine® in a 1:4 DCM to water mixture (total volume 5 mL, 53% combined API). The sample was emulsified using a Hielscher UP400S ultrasonic processor equipped with H7 Probe at 100% output (22 W) for 15–20 sec. Immediately after emulsification, the sample was spray dried on a benchtop spray dryer (BUCHI Mini-290) using an air-atomizing nozzle and compressed air as the drying gas. Spray drying process conditions were 5 mL/min solution flow rate and 65°C outlet temperature (120°C inlet temperature). The orange powder was collected and stored in the dark at room temperature.

Preparation of emulsion-spray-dried 52% TRIPLE drug powders containing RIF, INH, PZA labelled with 1% of the dye DiD (TRIPLE SDN + DiD)

Preparation followed the same procedure as described previously; however, a stock solution of 53-mg/mL DiD was prepared. A mass of 50.7-mg PZA, 19.8-mg RIF, and 8.7-mg INH were weighed directly into a sample vial. A volume of 97-mL DCM was then added and the powders mixed. To this, 0.03 mL of DiD stock was added. The aqueous stock solutions were added to the 1-mL API mix in DCM in the ratio 267:0.44 (mL) plus 0.89-mL water. The final solid mass ratio was therefore 33.7% PZA, 13% RIF : 6% IZH : 1% DiD : 40% Kollicoat® Protect : 7% Hyamine® in a 1:4 DCM to water mixture (total volume 5 mL, 52% combined API, 1% DiD).

Preparation of emulsion-spray-dried 30% DUAL drug powders containing RIF, INH

Preparation followed the same procedure as described previously for the TRIPLE SDN; however, 40-mg RIF and 20-mg INH were weighed directly into a sample vial. Stock solutions of Kollicoat Protect® (45 mg/mL in water) and Hyamine® (45 mg/mL in water) were dissolved. The aqueous stock solutions were added to the 1-mL API mix in DCM in the ratio 5.34-mL Kollicoat Protect® : 0.88-mL Hyamine® plus 1.78-mL water. The final solid mass ratio was therefore 20% RIF : 10% IZH : 60% Kollicoat Protect® : 10% Hyamine® in a 1:4 DCM to water mixture (total volume 5 mL, 30% combined API).

Powder X-ray diffraction

RIF SDNs were stored at 25°C in their powder, monolith form for 1 month at 25°C. Analysis was carried out by powder X-ray diffraction (p-XRD). p-XRD measurements were collected in transmission mode on solid monolith samples held on a thin Mylar film in aluminium well plates on a Panalytical X'Pert PRO MPD instrument with X'PERT OPERATOR INTERFACE (version 1.0b) software.

SDN preparation and characterisation

All SDNs were sub sampled under sterile conditions and kept in the dark at ambient temperature until use. SDNs were diluted in sterile 2% (vol/vol) foetal calf serum (prepared in sterile distilled water) at a concentration of 1 mg/mL and vortexed and then placed on ice. SDNs were then diluted in Middlebrook 7H9 broth supplemented with 10% (vol/vol) Middlebrook ADC enrichment (albumin/dextrose/catalase (Becton Dickinson, UK)), 0.2% (vol/vol) glycerol, 2-μg/mL mycobactin J (7H9). Agglomeration status, Zeta potential, and hydrodynamic sizes were analysed by dynamic light scattering (DLS) using plastic disposable cuvettes at an SDN concentration of 100 μg/mL using a Zetasizer Nano-ZS instrument (Malvern Instruments Ltd., UK). Each sample was measured in triplicate.

Reporter strain of Mycobacteria

The *Map* K10/GFP strain transformed with a plasmid carrying the *gfp* gene (and a kanamycin resistance gene), which allows growth and viability to be tracked with fluorescence, was kindly provided by Professor Raul Barletta, University of Nebraska, Lincoln (Harris *et al.* 2002). *Map* K10/GFP was cultured in Middlebrook 7H9 broth supplemented with 10% (vol/vol) Middlebrook ADC enrichment (albumin/dextrose/catalase (Becton Dickinson, UK)), with 0.2% (vol/vol) glycerol, 0.05% (vol/vol) Tween 80, 2-μg/mL mycobactin J, and 25-μg/mL of kanamycin (7H9K⁺) at 37°C gently stirred (250 rpm) continuously with magnetic stirrers.

Screening the antimicrobial properties of SDNs

The antimicrobial properties of SDNs and aqueous drugs were screened using the previously described assay (Donnellan *et al.* 2015). Briefly, *Map* K10/GFP was cultured in 7H9K⁺ until the exponential stage of growth. Sterile, black, 96 well plates (Nunc, Thermo Fisher) were seeded with *Map* K10/GFP (2 × 10⁶ CFU/100 μL/well). The bacteria were then exposed to SDNs and aqueous drugs in 7H9 at concentrations ranging from 1.875 ng/mL to 4 μg/mL (final 200 μL volume per well) and incubated for up to 7 days at 37°C with medium agitation (250 rpm) in the dark. Blank wells, medium only (no bacteria, no SDN/drug) and SDN/drug (no bacteria) were included as controls to check for SDN/drug interference. Fluorescence was measured using a GloMax® Multi+ plate reader

(Promega, UK) (Ex/Em 490/510–570 nm). Bacterial fluorescence was monitored immediately after SDN/drug addition (day 0), then at the same time each day for 7 days. All experiments were performed in triplicate, a minimum of three times, under sterile conditions.

Data analysis

Results expressed in arbitrary fluorescent units against time (days) were transformed and normalised to obtain a standard dose response relationship for comparison between SDNs and aqueous RIF using a data analysis protocol for screening the efficacy of antimycobacterial substances as previously described (Donnellan *et al.* 2015), where G is the fluorescent units, G_0 is the bacterial growth at time 0, β is the growth rate (per day), and t is the time (days).

Phage amplification assay

Detection and enumeration testing was carried out according to Rees and Botsaris (2012). Briefly, to perform the phage amplification assay, cell culture samples (200 μL) was mixed with 800-μL Middlebrook 7H9 broth supplemented with ADC and $CaCl_2$ (2 mmol/L). Samples (1 mL) containing mycobacteria were mixed with 1×10^8 mycobacteriophage D29 (100 μL) and incubated for 1 h. Remaining extracellular phage were then inactivated using a virucide treatment (100 μL 10 mmol/L ferrous ammonium sulphate for 6 min). The virucide was then neutralised by dilution using 5-mL Middlebrook 7H9 broth, and the phage-infected cells were plated in a lawn of fast growing *Mycobacterium smegmatis* (1 mL, 10^7 cfu/mL) using soft agar (0.8% *w/v*). Lysis of the infected cells at the end of the lytic cycle leads to the formation of plaques in the lawn of *M. smegmatis*. Because each plaque formed represents one mycobacterial cell in the original sample the assay can be used to enumerate the mycobacterial cultures (data reported as pfu/mL).

Cytotoxicity testing

Cytotoxicity of the SDNs on macrophages was assessed using the Alamar Blue® assay, a cell viability test by measuring mitochondrial activity. Macrophages (murine macrophage cell line J744A.1) were cultured in $75cm^2$ T5 flasks in complete medium (RPMI 1640 (Thermo Fisher Scientific, UK) supplemented with 10% heat inactivated foetal calf serum, 100-μg/mL streptomycin, 100-IU/mL penicillin, 0.1-mmol/L nonessential amino acid, 1-mmol/L sodium pyruvate solution) and incubated at 37°C, 5% CO_2 until 95% confluent. Cells were

harvested using a gentle scraping method under sterile conditions and resuspended in 6 mL of RPMI, centrifuged at 850 *g* for 5 min then seeded at a density of 5×10^4 cells/well into flat-bottomed, cell culture 96 well plates in a total volume of 100 μL per well. The plates were incubated at 37°C, 5% CO_2 for 24 h. SDN/drugs at a concentration range up to 8 μg/mL (each concentration was prepared in triplicate treatment groups) were added and incubated at 37°C, 5% CO_2 for a further 24 h. Positive (macrophages and 0.1% Triton (to indicate 100% of lysis of cells)) and negative (macrophages and medium only) controls were included in each plate. Following incubation, the supernatant was removed, cells were washed twice with 200 μL of PBS, and 0.1 mg/mL of Alamar Blue® reagent was added to each well and incubated for a final 4 h at 37°C, 5% CO_2, whereby fluorescence was read at an ex wavelength of 560 nm and an em wavelength of 590 nm using a SpectraMax M5 plate reader (USA). To determine if any SDN/drug interference occurred, the 96 well plate was centrifuged at 850 *g* for 2 min, and the supernatant was removed from each well and transferred into a fresh plate and reread.

Infection of macrophages with pathogenic *Mycobacterium*

Macrophages were detached from flasks using TrypLE™ and centrifuged at 850 *g* for 2 min before seeding into eight well chambered Permanox® slides (1×10^5 cells/well in a final volume of 200 μL) and incubated for 24 h at 37°C, 5% CO_2. Supernatant was removed from chambers, and cells were washed twice with 200-μL PBS. *Map* K10/GFP was cultured as described previously, and 10 mL of bacterial culture (in the exponential phase of growth) was centrifuged at 3090 *g* for 20 min and resuspended in 1 mL of PBS. The bacterial cell suspension was then centrifuged for 5 min at 670 *g* to remove any residual antibiotic (from the 7H9) and resuspended in 1 mL of PBS and passed through a Gilson tip several times to reduce clumping. Macrophages were infected with mycobacteria at a multiplicity of infection (MOI) of 30:1, 10:1, and 5:1 in complete medium (without streptomycin or penicillin) at a final volume of 200 μL per chamber (each MOI was performed in triplicate) and incubated for 4 h at 37°C, 5% CO_2. Supernatant was removed, and each chamber was washed twice with 200 μL of PBS to remove any residual/surface bound mycobacteria before fixing in 4% paraformaldehyde for 1 h. Control

chambers were subject to the same procedures and contained macrophages and medium only.

Imaging the uptake of SDNs by macrophages

Macrophages were prepared as outlined previously. SDNs with DiD incorporated were added to eight well-chambered Permanox® slides in complete medium (without streptomycin or penicillin) at a concentration range of 10–20 μg/mL in 200-μL final volume (each concentration performed in triplicate) to Map K10/GFP-infected and uninfected macrophages, which were incubated for a further 4 h at 37°C, 5% CO$_2$. Supernatant was removed, and each chamber was washed twice with 200 μL of PBS to remove any residual/surface bound SDNs and/or mycobacteria before fixing using 4% paraformaldehyde for 1 h. Control chambers contained macrophages and medium only and macrophages with fluorescent polystyrene bead NPs in medium (Molecular Probes, USA)).

Staining and fixed cell imaging of SDN treated and infected macrophages

Following fixation (using 4% paraformaldehyde for 1 h), macrophages were stained with 4′,6-diamidino-2-phenylindole dihydrochlodire (DAPI) nuclear stain (1:10 dilution in PBS). After 10 min, the slides were washed twice with distilled water before being mounted onto slides with Fluoro-Gel Mounting Medium with TES Buffer solution (EMS, USA). Cellular uptake was imaged using a Zeiss Axiovert 200M inverted Epi fluorescence microscope with an Axiocam MR3 camera using objective magnifications of 10×, 40×, 63×, and 100×. Cy3 (magenta, Ex/Em: 580/605 nm), Cy5 (yellow/red, Ex/Em: 596/670 nm), DAPI (blue, Ex/Em: 358/461 nm), GFP (green, Ex/Em: 488/507), and differential interference contrast or phase contrast channels (depending on objective) were used. Images were processed using IMAGE-J (Fiji) software (Schindelin et al. 2012) and ZEISS AXIO VISION REL 4.8 software (Z-stacks), thus showing the differential interference contrast (grey), DiD incorporated SDNs (red (RIF) and yellow (TRIPLE)), polyester beads (magenta), Map K10/GFP (green), and macrophage nuclei (blue).

Results and Discussion

SDN manufacture and screening

Solid drug nanoparticles of the first line TB antibiotics; RIF, RIF + INH (DUAL) and RIF + INH + PZA (TRIPLE) were synthesised and characterised via either an emulsion template freeze dried or emulsion spray dried method described previously (Giardiello et al. 2016; Zhang et al. 2008). Drug loading, size, and Zeta potential of the tested SDNs (in Middlebrooks 7H9 broth) are provided in Tables 1a and 1b. We also adapted two of the compounds (RIF and TRIPLE) to contain DiD (Table 1a), for imaging purposes. The drug/drug ratio of the loading was chosen to try and reflect what is used clinically (TRIPLE SDN) but with respect to maximising excipients wherever possible. A series of drug ratios were initially produced, and the drug combination that was the most reproducible was selected for this study. Excipients were required to stabilise the prespray of freeze drying, generally more excipient resulted in smaller particles (confirmed by DLS) by preventing particle growth and agglomeration. Specific excipients

Table 1a. Drug types and drug loading (%).

Drug/SDN	Total drug loading (%)	Formulation
RIF (rifampicin aqueous drug)	≥97	Powder[1] (stock suspension prepared with methanol)
INH (isoniazid aqueous drug)	≥99	Powder[2] (stock suspension prepared with distilled water)
RIF SDN (rifampicin solid drug NP)	30	30% RIF/55% F68® Protect/15% Hyamine®
TRIPLE SDN (rifampin, isoniazid, and pyrazinamide solid drug NP)	53.3	34% PZA/13% RIF/6% INH/40% Kollicoat® Protect/7% Hyamine®
DUAL SDN (rifampin, isoniazid solid drug NP)	30	20% RIF/10% INH/60% Kollicoat® Protect/10% Hyamine®

[1]Sigma-Aldrich® Product number R8883.

[2]Sigma-Aldrich® Product number I3377.

Table 1b. Dynamic light scattering (DLS).

SDN	Z-Average (d.nm)	Zeta potential (mV)	PdI
RIF	36.75 ± 6.34	−9.71 ± 0.38	0.77 ± 0.07
DUAL	40.73 ± 17.92	−7.49 ± 0.49	0.37 ± 0.01
TRIPLE	161.78 ± 8.56	−6.31 ± 0.86	0.31 ± 0.07
RIF + DiD	107.27 ± 32.93	−10.46 ± 0.47	0.56 ± 0.09
TRIPLE + DiD	415.3 ± 64.81	−10.43 ± 0.81	0.42 ± 0.03

Hydrodynamic diameter (Z-average), Zeta potential, and polydispersity index (PdI) of the SDN panel was assessed using DLS. Data expressed as mean ± SEM (n = 6) (temperature: 25°C, dispersant: Middlebrooks 7H9 broth, concentration 100 μg/mL, pH 6.9, equilibrium time: 30 sec). With or without 1,1′-dioctadecyl-3,3,3′,3′-tetramethylindodicarbocyanine, 4-chlorobenzenesulfonate salt (DiD).

(e.g., Pluronic F68®) were chosen based on their stability, determined by DLS.

The Z-Average diameter (nm) readings for the SDNs with DiD were larger than SDNs without the incorporated DiD dye, suggesting that those with the DiD dye either agglomerated more readily, or the dye incorporation increased the individual particle size (Table 1b). No statistical difference of the Zeta potential or dispersity was observed (Table 1b). Stability tests were conducted to confirm that RIF was stable by employing p-XRD. Relative to crystalline nonformulated RIF, RIF SDN was shown to be amorphous via p-XRD. Samples were stored for 4 weeks at 25°C and were shown to have remained amorphous over this period and not regressed back to their crystalline forms (Figure S1).

To investigate the bactericidal activity of the SDN formulations, as a surrogate for *Mtb*, we employed a green fluorescent protein (GFP) reporter strain of *Mycobacterium avium* subsp. *paratuberculosis* (*Map* K10/GFP) (Harris *et al*. 2002) permitting viability to be monitored using fluorescence. The antimycobacterial properties of the SDN formulations and aqueous preparations of RIF and INH (solubilised per product instructions) were assessed using the previously described assay (Donnellan *et al*. 2015). Viable *Map* K10/GFP (2×10^6 cfu/mL) was exposed to SDNs and aqueous drugs ranging in concentrations (0.001875–1.33 μg/mL) for 7 days. Following exposure to the SDNs the growth of *Map* K10/GFP was inhibited in a dose-dependent and time-dependent manner, but differing in efficacy between SDN types. The growth rates of *Map* K10/GFP were expressed as the change in fluorescence per day (β) (Donnellan *et al*. 2015) and plotted against drug concentration using the data modelling software GRAPHPAD (GraphPad, Prism 5®). For each compound, rather than comparing the total mass concentration

(for which mass includes polymer and/or surfactant), the molar equivalent of drug loading for all three SDNs was used (Fig. 1(A)). The IC_{50} was calculated for each compound: RIF SDN 0.02 μg/mL, DUAL SDN 0.17 μg/mL, and TRIPLE SDN 0.02 μg/mL; RIF aqueous 1.06 μg/mL, INH aqueous did not show an effect and therefore could not be calculated (potency ranking: RIF SDN = TRIPLE SDN > DUAL SDN > RIF aq > INH aq).

All compounds, except INH, induced a dose-dependent and time-dependent inhibition of *Map* K10/GFP growth (Fig. 1(A)). RIF, the backbone of TB therapy (Maartens and Wilkinson 2007; Longo *et al*. 2015; Laurenzo and Mousa 2011), as an SDN (containing 30% drug) was more inhibitory than aqueous RIF (Fig. 1(B)). Figure 1(B) demonstrates that by fitting the data using a three-parameter sigmoidal model, the RIF SDN exhibited improved potency (as demonstrated by the net reduction in control growth rate, i.e., the compound's kill rate) as evidenced by a 50-fold reduced IC_{50} value (0.02 μg/mL compared with 1.06 μg/mL) observed for the aqueous formulation. The efficacy between compounds at different time points (from day 0 to day 7) shows that RIF can also elicit a faster kill rate of *Map* K10/GFP when the drug is in the SDN form compared with a conventional aqueous solution (Table S1a,b). The INH formulated as the DUAL SDN, containing 10% INH and 20% RIF (Table 1a) or as an aqueous formulation, had little impact on the growth of *Map* as previously reported (Fig. 1(A)) (Williams *et al*. 1999; Krishnan *et al*. 2009). Although effective at killing *Mtb* and *M. bovis*, this prodrug requires activation via the product of the *katG* gene (catalase-peroxidase). This gene is found in *Map* (Granger *et al*. 2004) but may be down regulated in the K10/GFP strain, suggesting that the INH content contributed a relatively small inhibitory effect on mycobacteria growth (Fig. 1(A)). The TRIPLE SDN, which contained 34% PZA, 13% RIF, and 6%
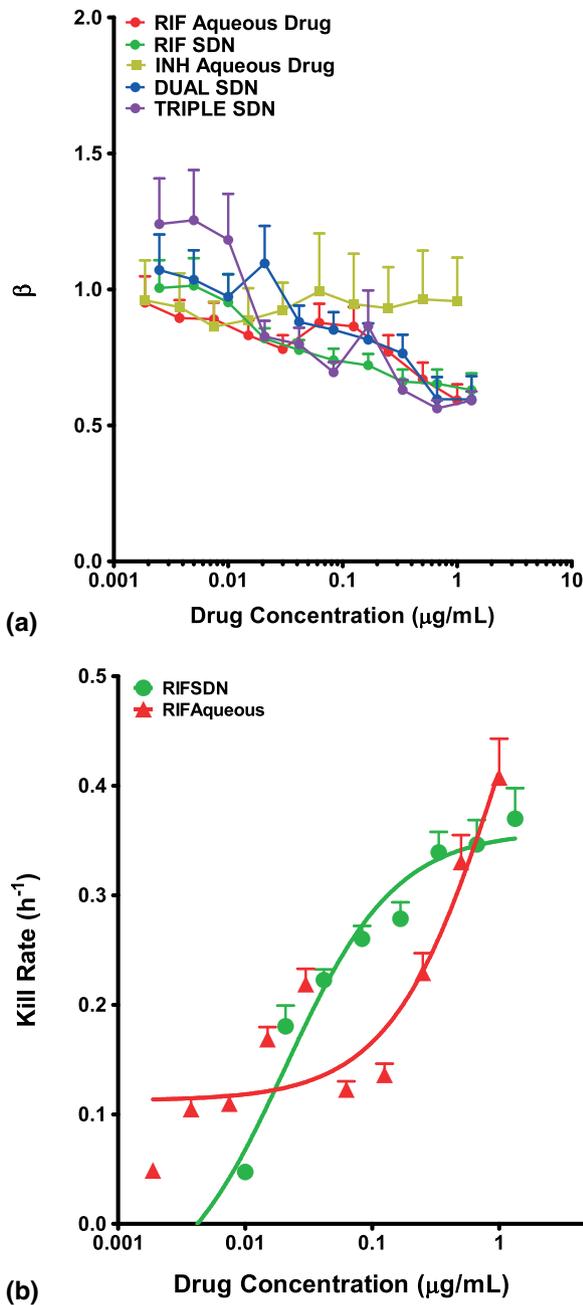
(a)

(b)

Figure 1. Normalised, transformed data showing the growth of *Map* K10/GFP grown in 7H9, in a microplate format, with SDNs and aqueous antibiotics at different concentrations (0.001875–1.33 μg/mL), normalised to the slope of the control where β represents the change in fluorescence (representing mycobacterial growth) per day. β was calculated through linear regression analysis of the change in fluorescence values over time for each concentration ($n \geq 3$). (B) Kill rate of RIF SDN Vs RIF aqueous against *Map* K10/GFP. Emax curves showing the relationship between the concentration of SDN or aqueous RIF and their corresponding kill rates. The kill rate at each concentration (0.001875–1.33 μg/mL) represents the net reduction in growth when compared to the corresponding control ($n \geq 3$).

INH (Table 1a) was as potent as the RIF SDN (IC_{50} 0.02 μg/mL). PZA is activated at an acidic pH during inflammation, and if phagocytosed by the macrophages, the SDN would be in an acidic environment. However, assessment of *Map* growth was performed in neutral conditions, which may suggest that this component of the SDN was relatively inactive and RIF exerted the dominant effect.

Infected macrophage SDN uptake

The next stage was to determine whether the SDNs could traffic to mycobacteria residing in macrophages. Firstly, we checked that the SDNs and aqueous RIF were not toxic to healthy macrophages (using the Alamar Blue® assay). The SDNs and drugs tested did not significantly affect cell viability ($P > 0.05$ (Figure S2)). We used fluorescence imaging to demonstrate uptake of both *Map* K10/GFP and SDNs and to determine if they colocalised to the same intracellular location of the cell. Macrophages were seeded (5×10^4 cells/well) and infected with mycobacteria at an MOI of 5:1, 10:1, and 30:1, then treated with SDNs incorporating DiD. Control experiments included macrophages only, macrophages treated with nontoxic, fluorescent 20 nm NP beads, and macrophages infected with *Map* K10/GFP only (Fig. 2(A–D)). Washing removed extracellular mycobacteria/SDNs/NPs beads prior to imaging. Figure 2(E–F) illustrates the uptake of fluorescent versions of the RIF and TRIPLE SDNs by macrophages. Z-stacks confirmed that RIF SDNs were distributed throughout the cell, both within the cytoplasm and nucleus (Figure S3a–g). The TRIPLE SDNs, being larger particles, appear to be agglomerated (consistent with the DLS data) with limited uptake by cells observed (Fig. 2(F)), which has been previously reported (Clift *et al*. 2008). Overall, it appears that SDNs remained as full, intact particles once engulfed by macrophages.

To determine localisation relative to mycobacteria, the fluorescent SDNs were administered to *Map* K10/GFP-infected macrophages. Figure 3(A) illustrates macrophages infected with *Map* K10/GFP (MOI of 10) treated with 20 μg/mL of RIF SDN. Both SDNs and mycobacteria were observed to be intracellular. To consolidate this finding, it was repeated with a lower SDN concentration and Z-stack images taken (Fig. 3(B)). The same test was carried out for the TRIPLE SDN (Fig. 3(C,D)). The mycobacteria and SDN appear to be colocalised for both SDN types, at least within the same 200-nm pixel area (the limit of image resolution).
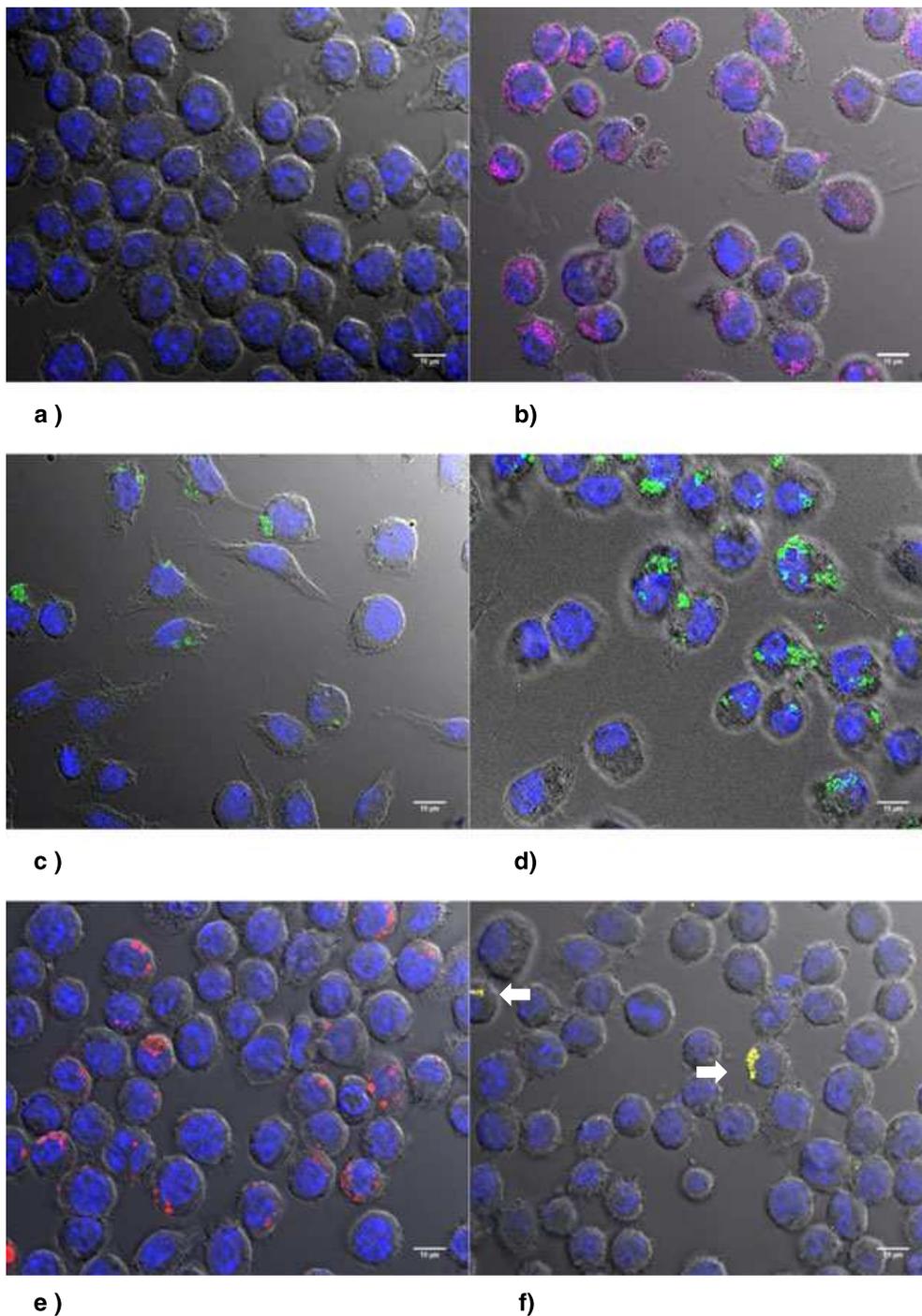
Figure 2. (A–F) Macrophage (J774A.1 murine macrophage cell line) treatments and infections. (DIC: grey, DAPI (nuclei): blue, NP beads (CY3): magenta, GFP (*Map*): green, far-red CY5 (SDNs): red and yellow, at 63× (scale bars all 10 μM)). (A) Macrophages (not infected or treated). (B) Macrophages treated with 10 μg/mL of NP beads. (C) Macrophages infected with *Map* K10/GFP at an MOI 5. (D) Macrophages infected with *Map* K10/GFP at a MOI 10. (E) Macrophages treated with 10 μg/mL of RIF SDNs. (F) Macrophages treated with 10 μg/mL of TRIPLE SDNs.

Because of the distance between GFP and far-red excitation (Ex)/emission (Em) peaks, wavelength crosstalk was unlikely to have occurred during the imaging. However, GFP and far-red signal crosstalk were tested for and found not to be occurring (Figure S4a,b). Therefore, we are confident that colocalisation of SDNs and mycobacteria does occur within macrophages.
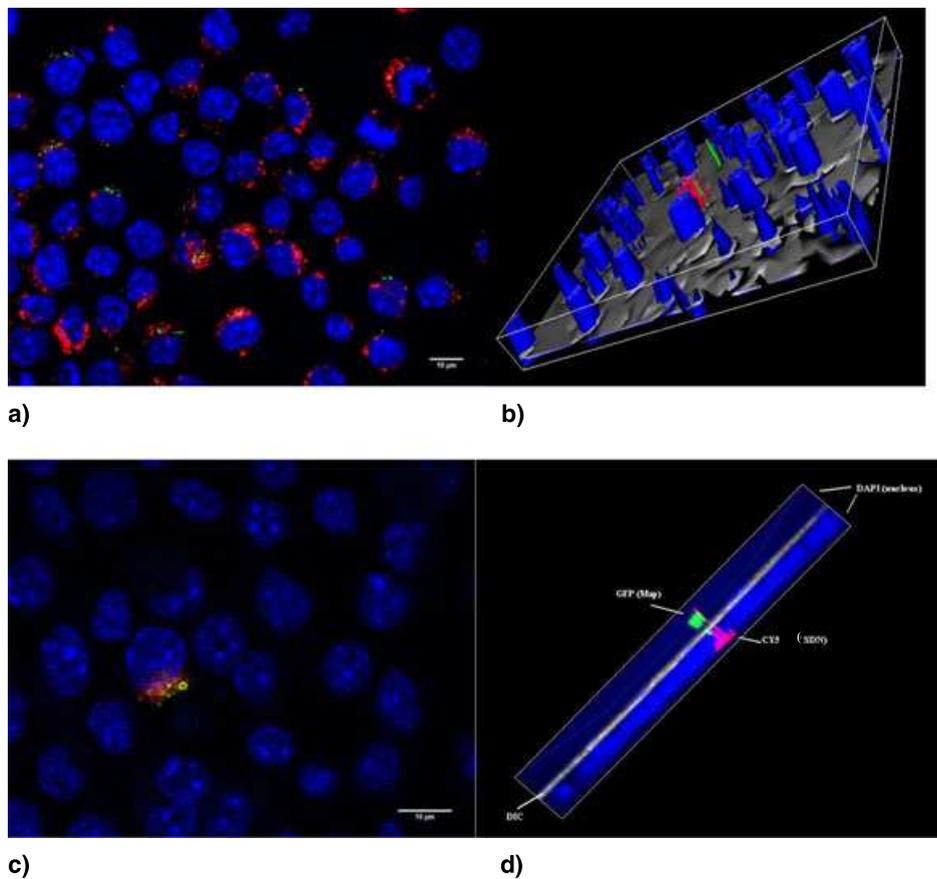
Figure 3. (A–D) Infected macrophages treated with RIF SDNs. (DIC: grey, DAPI (nuclei): blue, GFP (*Map*): green, far-red CY5 (SDNs): red and yellow, at 63× (scale bars all 10 μM)). (A) *Map* K10 GFP (MOI 10) infected macrophages following 4-h treatment with 20-μg/mL RIF SDN. (B) 3D image of *Map* K10/GFP (MOI 10) infected macrophages following 4-h treatment with 10-μg/mL RIF SDN with Z-stacks resorted using Zeiss Axio vision Rel 4.8. (C) *Map*/K10 GFP (MOI 10) infected macrophages following 4-h treatment with 10-μg/mL TRIPLE SDN where the yellow signal is indicative of two overlapping fluorescence signals, thus being indicative of colocalisation of SDNs and mycobacteria. (D) Z-stack resorted of Figure 3(C) using Zeiss Axio vision Rel 4.8. The different angles of the Z-stacks display the orientation of *Map* K10/GFP and further asserts the probable colocalisation of TRIPLE SDN and mycobacteria.
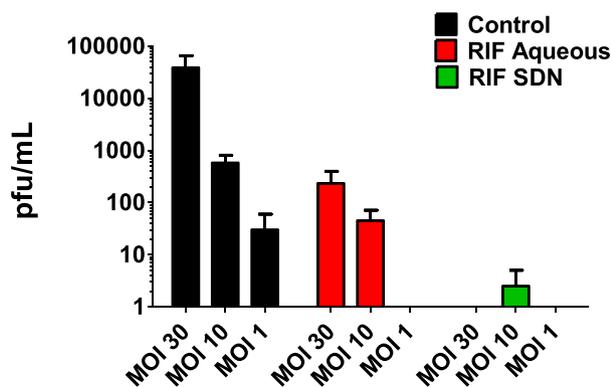

Figure 4. Phage amplification assay. Each plaque formed on soft agar represents one viable *Map* K10/GFP cell. Plaques were manually counted for each treatment type, at each MOI, following 24 h of treatment (each MOI carried out in triplicate, $n = 1$).

SDN versus aqueous drug intracellular potency

Our next objective was to determine the antimicrobial effects of the SDN within the infected macrophages. A preliminary study was carried out to compare the killing of *Map* K10/GFP by RIF SDN or aqueous RIF, within macrophages. Infected macrophages (MOI 1:1, 10:1 and 30:1) were exposed to each treatment for 24 h then lysed, and a phage amplification assay (Rees and Botsaris 2012) was performed. The results demonstrated that the mycobacteria were being killed by the drugs within the macrophages and that at an MOI of 10:1 and 30:1, RIF SDN was more potent to intracellular mycobacteria over the 24-h period than its aqueous counterpart (Fig. 4). Although an exciting initial result, further repeats in an intracellular model is required to consolidate this finding.

Conclusions

The main aims of novel drug discovery for TB are to lower effective drug dose and shorten the treatment period, which will consequently decrease costs and likelihood of resistance. This work aimed to address these factors. By working with FDA-approved drugs (RIF, INH, and PZA), excipients from the Inactive Ingredients Database (Kollicoat® protect, Hyamine®, and Pluronic F68®) and synthesising formulations of these drugs at the nano-scale, this approach may avoid the vast costs and timescales normally associated with novel drug development. Although SDNs would be viewed as novel drugs by the Medicines and Healthcare Products Regulatory Agency, as all the products are FDA approved, progression to clinical studies may be fast tracked. There are ongoing clinical trials of lopinavir and Efavirenz SDNs to treat HIV (Eudract number 2013-004913-41), thus showing the feasibility and potential of using SDNs to treat human diseases (Giardiello *et al*. 2016).

In summary, we have presented evidence, which shows that a nano-formulation of RIF is more effective (50-fold) than the conventional aqueous drug at killing a pathogenic *Mycobacterium* in vitro. We have verified that mycobacteria-infected macrophages can engulf SDNs, and both the drug and bacilli colocalise within macrophages. Nano-dispersions of drugs could be a more effective way of killing pathogens (Zhang *et al*. 2008; Choudhary and Kusum Devi 2015). Furthermore, we have demonstrated that we can synthesise dual-loaded and triple-loaded SDNs of FDA-approved anti-TB first line drugs, which would allow simultaneous delivery of the drugs in the multidrug treatment regime. Targeting drugs to macrophages, where the bacilli reside, is an important consideration in treating both active and latent TB infections because it can increase antimicrobial efficiency (Wang *et al*. 2014; Alexandru-flaviu and Cornel 2014). Our studies suggest that SDNs could offer an alternative, effective strategy for treating TB. This has important implications as it offers the potential to lower the dose and shorten the duration of treatment. In turn, this could lead to a reduction in treatment side effects and slow down the emergence of multidrug-resistant strains. Maintaining concentrations in target cells, with lower systemic concentrations, may help mitigate drug-to-druginteractions (a major problem faced when treating HIV and TB-coinfected patients) through lower hepatic exposure. The application of SDNs requires further investigation, but has the potential to become invaluable in treating infectious diseases worldwide.

Author contributions

K.S and V.S jointly conceived the project and obtained funding. S.D performed the experiments and wrote the manuscript. H.J provided laboratory support, C.W carried out the macrophage infection training, B.S carried out the phage assay training, A.O and S.R jointly conceived the SDN manufacture project, M.G manufactured the SDNs, and L.T and G.A analysed and interpreted the data. All authors discussed the results, conclusions and commented on the manuscript throughout the writing process.

Conflict of Interest

We declare no competing financial interests.

REFERENCES

Alexandru-flaviu, T., and Cornel, C. **2014**. Macrophages targeted drug delivery as a key therapy in infectious disease. Biotechnology, Molecular Biology and Nanomedicine *2*(1):19–21.

Bondarenko, O. et al. **2012**. Sub-toxic effects of CuO nanoparticles on bacteria: kinetics, role of Cu ions and possible mechanisms of action. Environ. Pollut. *169*:81–89.

Choudhary, S., and Kusum Devi, V. **2015**. Potential of nanotechnology as a delivery platform against tuberculosis: current research review. J. Control. Release *202*:65–75.

Clift, M. et al. **2008**. The impact of different nanoparticle surface chemistry and size on uptake and toxicity in a murine macrophage cell line. Toxicol. Appl. Pharmacol. *232*:418–427.

Donnellan, S. et al. **2015**. A rapid screening assay for identifying mycobacteria targeted nanoparticle antibiotics. Nanotoxicology *10*:761–769.

Giardiello, M. et al. **2016**. Accelerated oral nanomedicine discovery from miniaturized screening to clinical production exemplified by paediatric HIV nanotherapies. Nat. Commun. *7*:13184.

Granger, K. et al. **2004**. Recovery of Mycobacterium avium subspecies paratuberculosis from the natural host for the extraction and analysis in vivo-derived RNA. J. Microbiol. Methods *57*:241–249.

Harris, N. et al. **2002**. Cell sorting of formalin-treated pathogenic Mycobacterium paratuberculosis expressing GFP. Biotechniques *32*:522–527.

Krishnan, M. Y., Manning, E. J. B., and Collins, M. T. **2009**. Comparison of three methods for susceptibility testing of Mycobacterium avium subsp. paratuberculosis to 11 antimicrobial drugs. Journal of Antimicrobial Chemotherapy *64*:310–316.

Laurenzo, D., and Mousa, S. **2011**. Mechanisms of drug resistance in Mycobacterium tuberculosis and current status of rapid molecular diagnostic testing. Acta Trop. *119*:5–10.

Longo, D. L. et al. **2015**. Treatment of tuberculosis. New England Journal of Medicine *373*:2149-2160.

Maartens, G., and Wilkinson, R. **2007**. Tuberculosis. Lancet *370*:2030-2043.

Mcdonald, T. O. et al. **2014**. Antiretroviral solid drug nanoparticles with enhanced oral bioavailability: production, characterization, and in vitro-in vivo correlation. Adv. Healthc. Mater. *3*:400–411.

Mohanty, S. et al. **2013**. Cationic antimicrobial peptides and biogenic silver nanoparticles kill mycobacteria without eliciting dna damage and cytotoxicity in mouse macrophages. Antimicrob. Agents Chemother. *57*:3688–3698.

Neyrolles, O., Mintz, E., and Catty, P. **2013**. Zinc and copper toxicity in host defense against pathogens: mycobacterium tuberculosis as a model example of an emerging paradigm. Front. Cell. Infect. Microbiol. *3*:3–6.

Owens, B., **2013**. Nature News: Silver makes antibiotics thousands of times more effective. Nature News Article.

Pandey, R., and Ahmad, Z. **2011**. Nanomedicine and experimental tuberculosis: facts, flaws, and future. Nanomedicine: Nanotechnology, Biology, and Medicine *7*:259–272.

Pandey, R., and Khuller, G. K. **2005**. Solid lipid particle-based inhalable sustained drug delivery system against experimental tuberculosis. Tuberculosis *85*(4):227-234.

Patel, B. K., Parikh, R. H., and Aboti, P. S. **2013**. Development of oral sustained release rifampicin loaded chitosan nanoparticles by design of experiment. Journal of Drug Delivery *2013*:370938.

Pedrosa, P. et al. **2014**. Gold nanoprobes for multi loci assessment of multi-drug resistant tuberculosis. Tuberculosis (Edinb.) *94*(3):332–337.

Rees, C., and Botsaris, G. **2012**. The use of phage for detection, antibiotic sensitivity testing and enumeration. pp. 293-306. in P.-J. Cardona, ed. Understanding tuberculosis - global experiences and innovative approaches to the diagnosis. InTech, Rijeka.

Schindelin, J. et al. **2012**. Fiji: an open-source platform for biological-image analysis. Nat. Methods *9*:676–682.

Siccardi, M. et al. **2016**. Towards a rational design of solid drug nanoparticles with optimised pharmacological properties. Journal of Interdisciplinary Nanomedicine *1*:110-123.

Vadakkan, M. V. et al. **2013**. Dry powder cationic lipopolymeric nanomicelle inhalation for targeted delivery of antitubercular drug to alveolar macrophage. Int. J. Nanomedicine *8*:2871-2885.

Wang, B. et al. **2014**. Targeted drug delivery to intestinal macrophages by bioactive nanovesicles released from grapefruit. Molecular therapy: the journal of the American Society of Gene Therapy *22*:522-534.

WHO, **2015**. *Global TB Report 2015*.

WHO, **2014**. *Global Tuberculosis Report 2014*.

WHO, **2016**. *Global Tuberculosis Report 2016*.

Williams, P., Crauwels, H., and Basstanie, E. **2015**. Formulation and pharmacology of long-acting rilpivirine. Current Opinion HIV and AIDS *10*:233-238.

Williams, S. L., Harris, N. B., and Barletta, R. G. **1999**. Development of a firefly luciferase-based assay for determining antimicrobial susceptibility of Mycobacterium avium subsp. paratuberculosis. J. Clin. Microbiol. *37*:304-309.

Zhang, H. et al. **2008**. Formation and enhanced biocidal activity of water-dispersable organic nanoparticles. Nat. Nanotechnol. *3*:506–511.

Supporting information

Additional Supporting Information may be found online in the supporting information tab for this article.

Figure S1 RIF SDN stability test over 4 weeks at 25°C.

Figure S2 SDN/drug cytotoxicity to macrophages after 24 hr incubation.

Figure S3 Separated Z-stacks (a-f) and resorted Z-stacks of macrophages following 4 hr incubation with 10 μg/mL RIF SDN (g).

Figure S4 (a&b) 'Crosstalk test'

Table S1a Difference in bacteria growth between days when treated with RIF SDN.

Table S1b Difference in bacteria growth between days when treated with RIF aqueous.